

# Application of Fourier Analysis to Phase-Doppler-Signals Generated by Rough Metal Particles

THOMAS WRIEDT, KLAUS A. BAUCKHAGE, AND ARMIN SCHÖNE

**Abstract**—With the phase-Doppler-difference method the diameter and the velocity of spherical particles may be determined by measuring the frequency and the phase difference of burst signals detected by two or more photodetectors. In this paper a Fourier analysis method is described to extract frequency and phase information from the Doppler signals. The system is designed around a TMS320C25 signal processor board fitted into an AT computer. The performance of the frequency and phase estimator is examined. It is demonstrated that the method is particularly useful with noisy burst signals. Such signals may especially occur in investigating a metal spraying process.

## I. INTRODUCTION

THE PRODUCTION of dense metallic preforms directly from melt by spraying and deposition has become an attractive manufacturing method [1]. In this process the metal is converted into a spray of molten droplets by means of gas atomization. The spray impinges directly on a collecting surface to form a semifinished product. The spray process must be investigated on-line in order to be able to influence important process parameters and to control the mechanical properties of the preforms. To characterize the spray process the size and the velocity of the dispersed metal droplets have to be measured non-intrusively. This may be done by the well-known phase-Doppler-difference method [2].

A modified laser-Doppler-anemometer (LDVS) for simultaneous size and velocity measurements of individual spherical particles measures the velocity in the most familiar manner by detecting the frequency of the Doppler shift of the light scattered from a moving particle. The diameter of this particle is determined by detecting the phase difference between the two Doppler bursts received from two photodetectors situated at different angular positions parallel to the interesting velocity component of the particle. The overall setup of the dual beam system used is shown schematically in Fig. 1. It is the most common arrangement of a LDVS. The measuring volume is formed by the two interfering laser beams. It is an ellipsoid and may be interpreted by the fringe model also shown in Fig. 1. The edges of the ellipsoid are defined as the contour where the amplitude of the interference field

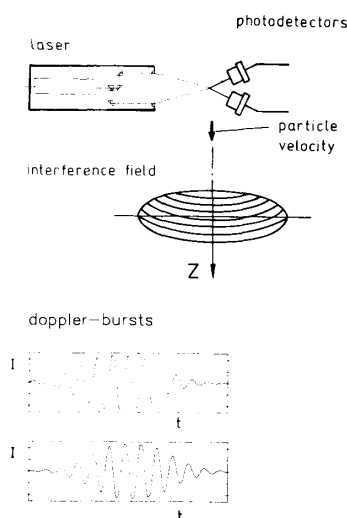


Fig. 1. Schematic of the LDVS method.

is  $e^{-2}$  of the maximum value. The signals detected by the photodetectors are generated by reflected or refracted fringes from a particle crossing the measuring volume. Accordingly the signals received by the two photodetectors have a frequency that varies with particle velocity.

Counters are the most common systems for processing phase-Doppler-difference signals. At normal measuring conditions that are at signal-to-noise ratios (SNR) of more than approximately 8 dB, they prove to be reliable [3]. However, under severe measuring conditions such as those occurring in metal spraying, counter processors will not work satisfactorily because of the poor quality of the signals detected by the photodetectors. Signal validation schemes are used to discard bursts of poor quality. The signals are especially influenced by background illumination and the rough surface of the particles. Rapid cooling of the metal particles gives rise to rough surface structures which result in diffuse reflections, and therefore, in noisy signals. Noise may also result from small particles, reduced laser power, poor light detectors, limited signal quantization, misaligned optics, or dusty process windows. At low SNR's spectral analysis provides better estimates of particle velocity than counters [4].

Different processors have been described using spectral analysis to estimate velocities of particles. Lading [5] in-

Manuscript received October 6, 1988; revised March 21, 1989. This work is an updated version of a paper presented at the International Conference on Laser Technologies in Industry, Porto, Portugal, June 1988.

The authors are with the Department of Production Technology, University of Bremen, FB 4, 2800 Bremen 33, Germany.  
IEEE Log Number 8929646.

roduced a burst spectrum analyzer based on a hard-wired fast Fourier transform (FFT) processor. Veynante and Candel [6] tested a nonlinear spectral analysis approach which hardly could be implemented in a real-time system. Neither of these processor schemes yields phase-difference information. In this paper a spectral analysis processor providing phase-difference and frequency information from the photodetector signals is described and its performance is evaluated with respect to the severe conditions of spraying and compacting molten metals. A similar system has lately been described by Domnick, Ertel, and Tropea [7]. Their system is based on a fast transient recorder and a personal computer to do the spectral analysis of the digitized burst signals. For on-line applications, however, it must be possible to identify the size and the velocity of quite a lot of particles in short time intervals. This is only possible by applying a special processor for computing the FFT of the burst signals. Such a system has been used by Maeda [8] to investigate a water spray flow by using the forward scattering mode.

## II. PROCESSING ALGORITHM

The spectral analysis processor is based on the FFT followed by an interpolation algorithm. The algorithm is divided into two parts. In a search routine the maximum spectral line is found. Then the approximate frequency estimate is improved by an interpolation scheme. Interpolation is essential because frequency resolution of the FFT is limited by the short duration of the bursts and the number of sampling points per burst. High computational speed requires a low number of sampling points. Different interpolation schemes have been published, e.g., least-mean-squares parabolic fit to the five FFT points nearest to the maximum [9], phase interpolation [10], and interpolation using all spectral components [11]. The true frequency and the phase of the signals may also be found by maximum likelihood estimation [12] combined with an offset FFT which has already been implemented on the TMS320C25 signal processor chip [13]. Because this would lead to a time consuming research routine, interpolation between spectral lines is favored.

In our case, for the phase-Doppler-method the line shape fitting method [14] is used to obtain exact values of frequency and phase from the spectral components computed by the FFT. The discrete Fourier transform  $X_n$  of the sampled signal  $x_k$  (the burst) is given by

$$X_n = \frac{1}{N} \sum_{k=0}^{N-1} x_k e^{-j2\pi kn/N}, \quad 0 \leq n \leq N-1 \quad (1)$$

with  $N$  being the number of sampling points and  $j$  the imaginary unit. The sampled data are supposed to satisfy the sampling theorem. The frequency resolution  $\Delta f$  in the frequency domain is given as a function of the sampling interval  $\Delta t$  by

$$\Delta f = \frac{1}{N\Delta t}. \quad (2)$$

Therefore, the maximum of  $|X_n|$  will not normally correspond to the frequency  $f$  and amplitude  $A$  of the periodic signal. If the signal frequency does not coincide with some spectral line  $f_n = n \cdot \Delta f$  "spectral leakage" will occur. This is because the "true" spectrum will be convoluted with the Fourier transform of the rectangular time window. The power of the signal leaks to spectral lines close to the true frequency.

Based on the assumption that the periodic signal is a sinusoid embedded in background noise, Rajaone [14] derived relations to interpolate between three spectral lines if a spectral peak is detected at the spectral line  $X_m$ . The interpolated frequency  $f_m$  is given by

$$f_m = \frac{m + \epsilon_m}{N\Delta t} \quad (3)$$

where

$$\epsilon_m = \text{Im} \left( \frac{j(B-1)}{B+1} \right) \quad (4)$$

and

$$B = \frac{X_m - X_{m+1}}{X_m - X_{m-1}}. \quad (5)$$

The corresponding phase  $\Phi_m$  may be calculated from the complex amplitude  $A_m$

$$\Phi_m = \text{arc}(A_m) \quad (6)$$

$$A_m = (2X_m - X_{m+1} + X_{m-1}) \frac{Z_m(Z_m^2 + 4\pi^2)}{8\pi^2(1 - e^{-Z_m})} \quad (7)$$

where

$$Z_m = \frac{j2\pi(B-1)}{B+1}. \quad (8)$$

The phase-difference corresponding to the size of the measured particle is obtained from the difference of the phases of the two burst signals.

## III. BLOCK DIAGRAM

The block diagram of the electronic system that is used for our evaluations is shown in Fig. 2. The signals from the photodetectors are amplified. The pedestal of the bursts is filtered out by the high-pass filters. The signal is low-pass filtered to remove high frequency noise. The outputs of the filters are applied to a burst detector which will load the buffer memory with the digitized signals after a burst amplitude is detected exceeding a suitable Schmitt trigger level. The sampling rate of the A/D converters is 28 MHz. The buffer memory is equipped with SRAM's 32 k × 8 bit working with 35-ns access time. The sampled signals are to be Fourier transformed by the TMS320C25 signal processor. The complex amplitudes of the maximum spectral line and the two lines nearby are

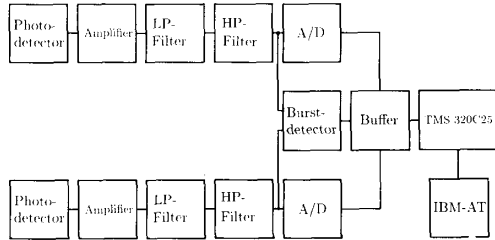


Fig. 2. Block diagram of the electronic system.

transferred to the IBM-AT computer which has to do the interpolation between the FFT bins. On the IBM-AT a Pascal programme is implemented which computes histograms of the particle velocity and size distributions.

The decision in favor of the TMS320C25 signal processor chip as a coprocessor was caused by its special applicability for mathematically intensive algorithms [15] and by the availability of fast FFT algorithms [16]. The TMS320C25 is the latest member of the TMS320 single-chip digital signal processor family. It provides a variety of options to carry out an FFT and has, therefore, found wide application in spectral analyzers, speech analysis, and instrumentation. A single 128 real value FFT may be executed in a single chip in about 1 ms. The chip utilizes a Harvard architecture with separate program and data memory spaces. A 16 bit  $\times$  16 bit hardware multiplier is incorporated to allow a multiplication to be executed in a single cycle. With the FFT the bit-reverse addressing mode is especially useful.

#### IV. VARIANCE BOUND OF THE ESTIMATES

With every measuring instrument or estimator a standard is helpful against which to judge the performance of the measurements or estimates. An estimate with a small bias and a small variance will be preferable. The bias may usually be neglected [17]. The discrete Fourier transform may be interpreted as a maximum-likelihood estimator of frequency and phase [17]. Maximum-likelihood estimates of signal parameters are unbiased at high SNR's.

The Cramér-Rao lower bound of the variance applies to an unbiased estimator. Even with some bias this bound may serve as a standard. It is commonly used as a performance standard. The Cramér-Rao lower bounds may be obtained from the Fischer information matrix. For the derivation the reader is referred to Rife [17]. The variance bound of the frequency estimator is given by

$$\sigma_f^2 = \frac{6}{(2\pi)^2 \text{SNR} \Delta t^2 N(N^2 - 1)}. \quad (9)$$

The bound for the phase estimator is given by

$$\sigma_\Phi^2 = \frac{2(N-1)(2N-1)}{\text{SNR} N(N^2 - 1)}. \quad (10)$$

SNR is the signal-to-noise ratio.

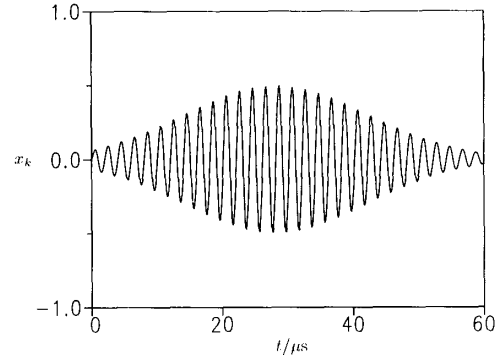


Fig. 3. Simulated burst signal without noise.

#### V. SIMULATION

To evaluate the performance of the proposed estimator the variance of the frequency and the phase estimates have been obtained by simulation. The burst signals have been generated by the following formula:

$$x_k = e^{-2(k\Delta t - T_B)^2/\sigma_B^2} \sin(2\pi f^k \Delta t) + w_k \quad (11)$$

with  $N_B$  being the number of periods in the burst and where

$$\sigma_B = \frac{0.5N_B}{f} \quad (12)$$

$$T_B = -\sigma_B \quad (13)$$

$$w_k = \sum_{m=1}^M \cos(2\pi f_{\max} m k \Delta t / M + \varphi_m). \quad (14)$$

This formula corresponds to the high-pass filtered signal detected by the photomultiplier. A second burst has been generated with a phase shift of 140 degrees. Half the duration time of the burst is given by  $\sigma_B$  corresponding to the amplitude which is  $e^{-2}$  of the maximum value. The frequency  $f$  of the simulated burst is 500 kHz. The number of periods in the burst is 28.

The bursts are sampled with  $\Delta t = 0.3035 \mu\text{s}$  and 128 sampling points have been used to calculate the Fourier transform.  $w_k$  is a Gaussian white noise process generated by the method given by Kafadar [18] as the sum of  $M = 2048$  cosine terms with uniformly distributed phase terms  $\varphi_m$ . This gives a flat noise spectrum with zero autocorrelation for all nonzero time shifts. The noise bandwidth  $f_{\max}$  used is 1 MHz, which satisfies the sampling theorem. In Fig. 3 one of the two synthesized burst signals having no noise component is plotted. Fig. 4 shows the same burst signal with a SNR of 6.5 dB.

About 100 realizations of a burst with the same SNR have been used to calculate the statistics of the frequency and phase estimates. In Fig. 5 the standard deviation of the frequency is plotted on a logarithmic scale as a function of SNR. In Fig. 6 the standard deviation of the phase-difference is shown. As can easily be seen, both the standard deviation of the estimated frequency and the standard deviation of the phase-difference compare quite well

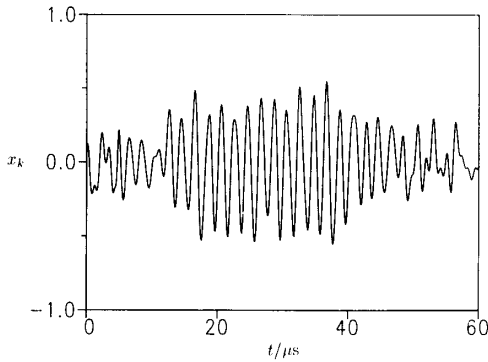


Fig. 4. Simulated burst signal with a SNR of 6.6 dB.

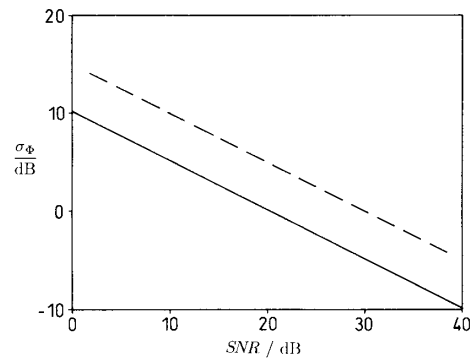


Fig. 6. Standard deviation of the phase-difference, — Cramér-Rao lower bound, --- simulation results.

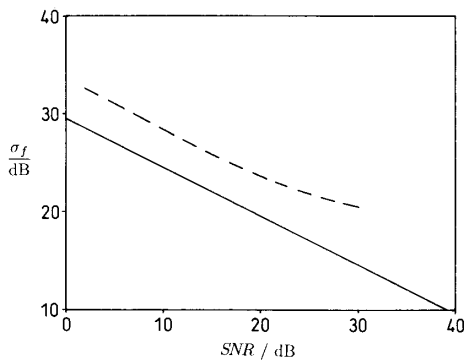


Fig. 5. Standard deviation of the frequency, — Cramér-Rao lower bound, --- simulation results.

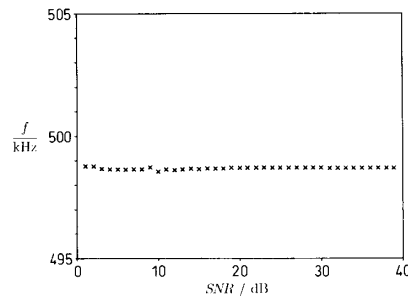


Fig. 7. Mean value of the frequency as a function of SNR.

with the Cramér-Rao bounds also plotted in both figures. The differences between the standard deviations which have been obtained by simulation and the corresponding bounds is just some decibels. This shows that the FFT method with the interpolation scheme indeed works for laser-Doppler signals which have a SNR of 0 dB.

In Figs. 7 and 8 the mean frequency and the mean phase-difference from analyzing about 100 burst signals with the same noise power are shown as a function of the SNR. The mean value of the frequency is nearly independent from the amount of noise in the burst signals. The bias from the true value is about 1 kHz which is 0.2 percent. Higher noise power leads to more bias with the phase-difference estimator as is shown in Fig. 8. The mean value of the phase-difference converges with increasing SNR to the true value of the phase-difference of 140 degrees. At a SNR of 10 dB, which is a realistic value with burst signals measured in metal spraying, the bias is about 2 degrees which is 1.4 percent, and therefore, lower than is possible by many counter processors at this SNR.

If the burst signals are not as noisy even one-bit quantization will give satisfactory measurement results. One-bit quantization will reduce the expense for the fast A/D converters and fast data memory space. With one-bit quantization the sampling rate may be increased ten fold with minor cost. Every digitization process introduces

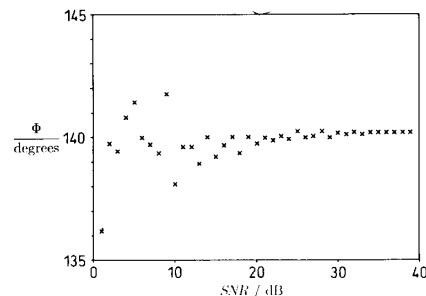


Fig. 8. Mean value of the phase-difference as a function of SNR.

quantization noise to the signal. The quantization noise is dependent on the number of quantization levels of the A/D converters used, the less levels used, the higher the quantization noise. The theoretical SNR for a sine wave quantized with one bit is 7.8 dB. For less than about four bits the effect of the quantization is to produce prominent noisy spectral lines which are harmonically related to the fundamental signal frequency [19]. With one-bit quantization the power of the highest noisy spectral line is about 10 dB lower than the power of the fundamental line.

In the next four figures the results of simulating one-bit quantization are given. In Fig. 9 the standard deviation of the frequency estimate is plotted as a function of the SNR of the burst and in Fig. 10 the standard deviation of the phase-difference estimate is given. Compared to Figs. 5

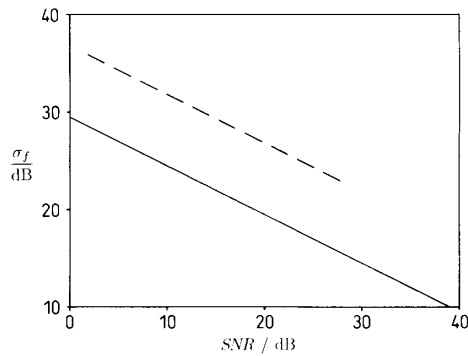


Fig. 9. Standard deviation of the frequency, — Cramér-Rao lower bound, --- simulation results obtained by using one-bit quantization.

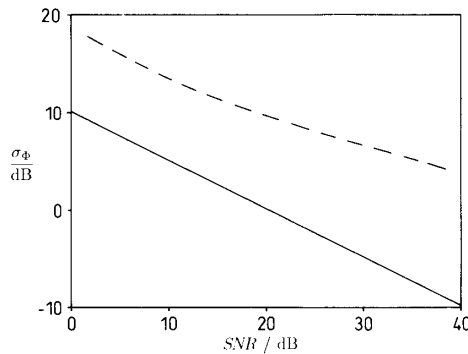


Fig. 10. Standard deviation of the phase-difference, — Cramér-Rao lower bound, --- simulation results obtained by using one-bit quantization.

and 6 both plotted curves are shifted to the right because the SNR of the processed bursts is decreased by the one-bit quantization. Therefore, both standard deviations are about 3 dB worse than the standard deviations obtained above. Fig. 11 shows that down to a SNR of 10 dB the frequency estimate is correct to 0.2 percent of the true value. From Fig. 12 one can conclude that the phase-difference estimate at a SNR of 10 dB is correct to 2.5 percent. These results of simulating one-bit quantization show the advantage of processing LDVS signals in the frequency domain.

#### VI. APPLICATION OF THE SPECTRAL ANALYSIS PROCESSOR TO POWDER METAL SPRAYS

On principle the applicability of the phase-Doppler method is limited to the diagnosis of spherical particles only. However, spherical shape in this context is a question of interpretation, i.e., the limitation of the method depends highly on the extent of deformation of shape or on the roughness of the particle surface. Thus the recognizability of spherical particles is not necessarily limited to fluid droplets with smooth surfaces caused by surface tension. Solidification processes of molten metals or highly concentrated solutions may influence the surface of the spherical particles as illustrated in Fig. 13. Shrink-

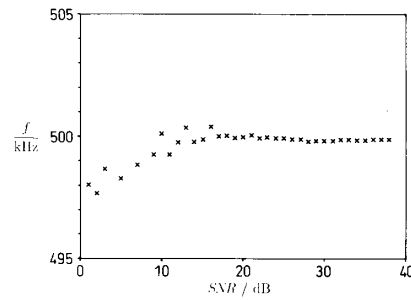


Fig. 11. Mean value of the frequency as a function of SNR obtained by using one-bit quantization.

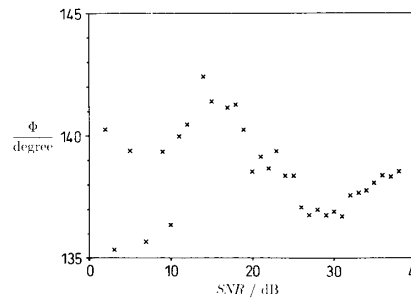


Fig. 12. Mean value of the phase-difference as a function of SNR obtained by using one-bit quantization.

ing effects of the surface "skin" in this case are caused by dendritic crystallization processes under rapid quenching boundary conditions. After changing the process parameters also, amorphous material structures may be generated, which also in most cases in our research work do not necessarily prevent particle size measurements. Of course, the quality of the Doppler bursts gets worse if spherical particles with rough surface structures give rise to diffuse reflection. However, as will be seen, the FFT improves the success of signal processing in a decisive manner. This means that for compaction processes as described recently [20], [21], LDVS measurements can be taken from the two-phase flow in the spray cone starting shortly downstream from the atomizer and ending at least directly above the substrate or deposit. All spherical particles can be measured, liquid and already solidified ones, also slightly deformed spheres like those in Fig. 13.

To demonstrate the performance of the described FFT method two CuAl particles have been analyzed both by a common LDVS-counter processor and by the FFT method. In order to guarantee controlled measuring conditions the particles have been mounted on a turning table revolving with a constant speed through the measuring volume. The number of sampling points is 128 and the sampling interval is  $0.4 \mu\text{s}$ . Both particles are extremely nonspherical and have a rough surface. Therefore, the signals differ from their ideal form, as can be seen in Figs. 14 and 15. In these figures the two burst signals resulting from one of the measurements of the second particle are plotted. Because of their irregular shape the burst signals

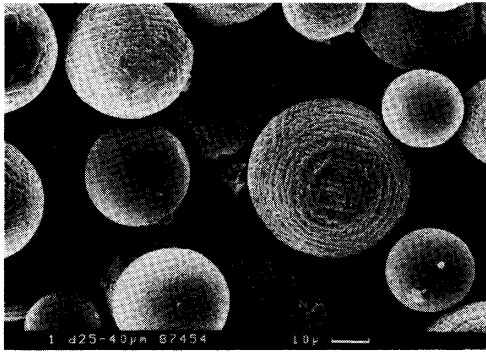


Fig. 13. Electron microscopic photo of steel spheres with different surface structures.

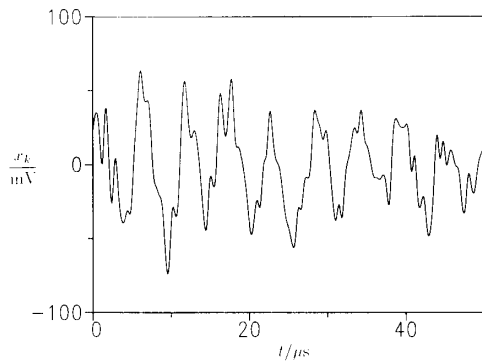


Fig. 14. First sample burst of the third measurement of particle 2 of Table 1.

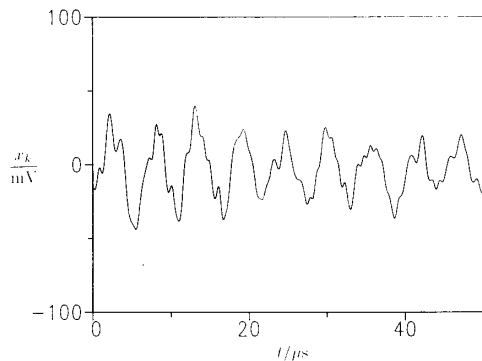


Fig. 15. Second sample burst of the third measurement of particle 2 of Table 1.

resulting from this particle could not be analyzed with the counter-method. The discrete Fourier transforms of these two burst signals which are utilized by the FFT method are shown in Figs. 16 and 17. In both transforms there is a significant peak which can easily be detected by the search routine of the FFT method. High noise power of the time signals may be deduced from the other peaks in the diagram of the Fourier transform. In Table I the results of the measurements are tabulated. Because of the nonsphericity of the investigated particles they cannot be

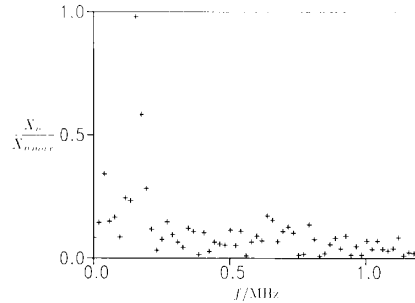


Fig. 16. Computed discrete Fourier transform of the signal of Fig. 14.

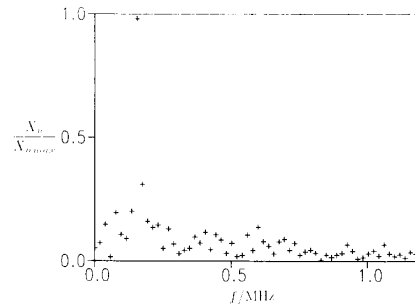


Fig. 17. Computed discrete Fourier transform of the signal of Fig. 15.

TABLE I  
COMPARISON OF MEASURED RESULTS FROM ANALYZING TWO CuAl PARTICLES BY THE LDVS COUNTER AND THE FFT METHOD

method	microscopic		LDVS-counter		FFT-method		
	v/m/s	d <sub>1</sub> /μm	d <sub>2</sub> /μm	v/m/s	d/μm	v/m/s	d/μm
1	2.24	45	225	2.24	28.2	2.24	31.9
1	2.24	45	225	2.25	27.4	2.24	33.0
1	2.24	45	225	2.25	29.9	2.24	33.4
1	2.24	45	225	2.25	31.9	2.24	33.4
2	1.95	45	135	-	-	1.96	69.4
2	1.95	45	135	-	-	1.96	72.6
2	1.95	45	135	-	-	1.95	69.9

described by just one diameter and accordingly two orthogonal diameters  $d_1$ ,  $d_2$  have been obtained by microscopic inspection.

The measurements of the velocity differ only slightly from the speed of the revolving table. The size measurements of the first particle by the counter and the FFT method lead to practically the same results. The second particle could only be analyzed by the FFT method which gives the correct velocity. The measured diameter of the particle may lead to interpretation because it is highly nonspherical but gives a correct indication of the particle size.

### VII. CONCLUSION

It was shown that special digital spectral analysis methods using FFT combined with an interpolation technique in LDVS measurements give good estimates of particle size and velocity even under bad measuring conditions. This was specifically investigated for the conditions in spray cones of droplets of molten and solidifying metals.

## REFERENCES

- [1] R. W. Evans, A. G. Leathan, and R. G. Brooks, "The Ospray preform process," *Powder Metallurgy*, vol. 28, no. 1, pp. 13-20, 1985.
- [2] K. Bauckhage, "The phase-Doppler-difference-method, A new laser-Doppler technique for simultaneous size and velocity measurement," Part 1, *Part. Part. Syst. Charact.*, vol. 5, pp. 16-22, Mar. 1988.
- [3] J. A. C. Humphrey, A. Melling, and J. H. Whitelaw, "Laser-Doppler anemometry for the verification of turbulence models," in *Proc. Conf. Engineering Uses Coherent Optics*, Strathclyde Univ., 1975.
- [4] L. Lading, "Spectral analysis versus counting," in *Proc. Int. Symp. Laser Anemometry*, ASME, FED, vol. 33, pp. 186-196, 1985.
- [5] —, "Spectrum analysis of LDA signals," in *Proc. Int. Specialists Meeting 'The Use of Computers in Laser Velocimetry'*, Saint-Louis, pp. 20.1-13, 1987.
- [6] D. Veynante and S. M. Candel, "Promising approach in laser Doppler velocimetry data processing: Signal reconstruction and nonlinear spectral analysis," *Signal Proc.*, vol. 14, pp. 295-300, 1988.
- [7] J. Domnick, H. Ertel, and C. Tropea, "Processing of phase/Doppler signals using the cross spectral density function," in *Proc. Fourth Int. Symp. Applications Laser Anemometry to Fluid Mechanics*, pp. 3.8.1-6, Lisbon, Portugal, July 1988.
- [8] M. Maeda, N. Sanai, K. Kobashi, and K. Hishida, "Measurement of spray mist flow by a compact fiber LDV and Doppler-shift detector with a fast DSP," in *Proc. Fourth Int. Symp. Applications of Laser Anemometry to Fluid Mechanics*, pp. 6.8.1-6, Lisbon, Portugal, July 1988.
- [9] R. F. Barrett and D. R. A. McMahon, "Comparison of frequency estimators for underwater acoustic data," *J. Acoust. Soc. Amer.*, vol. 79, pp. 1461-1471, May 1986.
- [10] D. R. A. McMahon and R. F. Barrett, "An efficient method for the estimation of the frequency of a single tone in noise from the phases of discrete Fourier transforms," *Signal Proc.*, vol. 11, pp. 169-177, 1986.
- [11] A. Zavaljevski and G. Zivanovic, "A technique for frequency estimation using FFT," in *Proc. MELECON '85*, vol. 2, pp. 41-44, 1985.
- [12] D. W. Tufts and R. Kumaresan, "Improved spectral resolution 2," in *Proc. Int. Conf. Acoustics, Speech, Signal Processing*, pp. 592-596, 1980.
- [13] G. Wade, "Offset FFT and its implementation on the TMS320C25 processor," *Microprocessor and Microsystems*, vol. 12, no. 2, pp. 76-82, 1988.
- [14] R. D. Rajaona and P. Sulmont, "A method of spectral analysis applied to periodic and pseudoperiodic signals," *J. Comput. Phys.*, vol. 61, pp. 186-193, 1985.
- [15] K. S. Lin, G. A. Frantz, and R. Simor, "The TMS320 family of digital signal processors," *Proc. IEEE*, vol. 75, pp. 1143-1159, 1987.
- [16] P. Papamichalis and J. So, "Implementation of fast Fourier transform algorithms with the TMS 32020," in *Digital Signal Processing Applications with the TMS320 Family*. Houston, TX: Texas Instruments Inc., 1986.
- [17] D. R. Rife and R. R. Boorstyn, "Single-tone parameter estimation from discrete-time observations," *IEEE Trans. Inform. Theory*, vol. IT-20, pp. 591-598, Sept. 1977.
- [18] K. Kafadar, "Gaussian white noise-generation for digital signal synthesis," *IEEE Trans. Instrum. Meas.*, vol. IM-35, pp. 492-495, 1986.
- [19] A. Sowards, "Introduction to d.s.p.," *Electron. Wireless World*, vol. 94, no. 1630, pp. 741-746, 1988.
- [20] K. Bauckhage, P. Schreckenberger, and H. Vettors, "Atomization of liquid metals by pressure gas-ring nozzles, A new application of spray systems for spray compacting materials with enhanced properties," in *Proc. 4th Int. Conf. Liquid Atomization and Spray Systems, ICASS-88*, pp. 215-219, Sendai, Japan, Aug. 1988.
- [21] K. Bauckhage, H.-M. Liu, and U. Fritsching, "Models for the transport phenomena in new spray compacting process," in *Proc. 4th Int. Conf. Liquid Atomization and Spray Systems ICASS-88*, pp. 425-430, Sendai, Japan, Aug. 1988.